Mixed convection in a lid-driven cavity: Appearance of bifurcation, periodicity and hysteresis

M. D. Deshpande[1,2,*] and B. G. Srinidhi[1]

[1]Computational and Theoretical Fluid Dynamics Division, National Aerospace Laboratories, Bangalore 560 017, India
[2]Present address: M.S. Ramaiah School of Advanced Studies, Bangalore 560 054, India

Mixed convection in a rectangular parallelepiped has been studied by solving the Navier–Stokes and the energy equations. The convective motion may show a time periodic behaviour for certain combinations of the parameters, even though the boundary conditions are steady. Further, certain features of dynamical systems like bifurcation, hysteresis and period doubling are also seen.

Keywords: Bifurcation, hysteresis, mixed convection, Nusselt number, periodicity, period doubling, Rayleigh number.

WE report here some interesting results regarding mixed thermal convection in a rectangular parallelepiped. Apart from possible natural convection due to differential heating, the fluid is also set into motion by the motion of the top lid of the container (Figure 1), which moves in its own plane. These two mechanisms of buoyancy (Rayleigh number Ra is a measure) and forcing by the lid motion (Reynolds number Re is a measure) lead to complex interaction[1–3].

Depending on the values of Re and Ra, the flow inside the cavity may be: no flow ($Re = 0$, $Ra < Ra(\text{crit})$), steady, periodic, quasiperiodic or turbulent. This critical value of Ra to set the motion when there is no forcing due to the lid motion has been calculated numerically. Also, the flow has been mapped to identify the various regimes. More interestingly, we have been able to detect periodic solutions for a select combination of these two parameters. Further, the features of a classical dynamical system like bifurcation, period doubling, hysteresis and chaos usually observed in phase space have been observed in physical space itself.

Formulation of the problem and numerical solution

The geometry of the rectangular parallelepiped and the coordinate axes are shown in Figure 1. The x-direction is measured downward along gravity g. The lid moves with a constant velocity v_0' in its own plane along the y-direction. The dimensions of the container are l_x', l_y' and l_z'. All lengths are non-dimensionalized using l_x' and velocities using $v'_{\text{ref}} = \nu/l_x'$. ($\nu$ is the viscosity, ρ the density of the fluid). Non-dimensional variables are indicated without a prime. Then $l_x = 1$. In this study we take $l_y = 1$ and spanwise aspect ratio, SAR = $l_z = 3$. The four vertical side walls are insulated and the no-slip velocity boundary condition is maintained at all the six walls. The governing equations are the continuity, Navier–Stokes and energy equations with the Boussinesq approximation[4].

Other non-dimensional variables are time $\tau = t\nu/(l_x')^2$, pressure $p = p'/[\rho(v'_{\text{ref}})^2]$, temperature $\theta = (T' - T_0')/\Delta T'$, $Re = (v_0' l_x'/\nu) = (v_0'/v_{\text{ref}}')$ = speed ratio of the lid, Prandtl number $Pr = \mu c_p/k$, $Ra = g\beta \mid T_2' - T_1' \mid l_x'^3/(\nu\alpha)$. The value of Pr is kept at 7 to match the value for water taken in Prasad and Koseff[3]. The governing equations are:

$$D = \nabla . \vec{u} = 0, \tag{1}$$

$$\frac{\partial \vec{u}}{\partial \tau} + (\vec{u}.\nabla)\vec{u} = -\nabla p + \nabla^2 \vec{u} - \hat{e}_x \frac{Ra}{Pr}\theta, \tag{2}$$

$$\frac{\partial \theta}{\partial \tau} + (\vec{u}.\nabla)\theta = \frac{1}{Pr}\nabla^2 \theta. \tag{3}$$

Instead of eq. (1), we solve a Poisson equation for p:

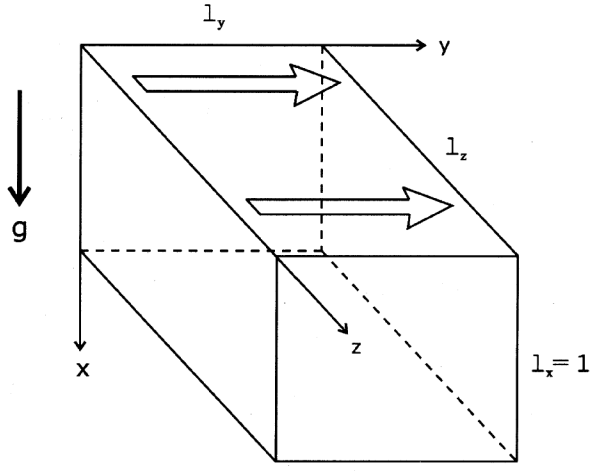

Figure 1. Geometry of the cavity.

*For correspondence. (e-mail: deshpande@msrsas.org)

$$\nabla^2 p = -\frac{\partial D}{\partial \tau} - \nabla.[(\vec{u}.\nabla)\vec{u}] + \nabla^2 D - \frac{Ra}{Pr}\frac{\partial \theta}{\partial x}. \quad (4)$$

Equations (2) and (3) are solved by the well-known Marker and Cell (MAC) method on a staggered grid[5]. An important improvement adopted here is the third-order upwind scheme[6], which has good stability characteristics and maintains at the same time, third-order accuracy of the convective terms. In the staggered grid arrangement, pressure and temperature are stored at the cell centre and at the centre of each face of the cell is specified the velocity component normal to the face. Equations (2) and (3) are solved by time marching using the Euler explicit scheme and eq. (4) for p is solved iteratively by over-relaxation. A central difference scheme is used to approximate all the terms except the convective terms. To maintain this high accuracy, boundary conditions are also approximated by second-order schemes. Thus, the overall accuracy of the numerical scheme is second order in space and first order in time.

The computational procedure has been tested extensively and some of the results are reported in Deshpande[7]. Grid independence studies and tests to check the adequacy of other computational parameters like time increment $\Delta\tau$, have been conducted successfully. The results for the classical Rayleigh–Benard problem[4,8] were also reproduced successfully. Based on these tests, a $(44 \times 44 \times 124)$ uniform, cartesian grid was found to be quite adequate for this study. Comparison with the results of Chiang *et al.*[9], as seen in Figure 2, is satisfactory even though there is a localized discrepancy of about 6% in the maximum velocity around, $y = 0.7$.

Results and discussion

Numerical calculations have been carried out for six values of $Re = 0$, 1, 50, 100, 200 and 400 and for a large number of combinations of Re and Ra. We will present here some sample results to describe different flow regimes, but concentrate on only two values of $Re = 50$ and 200 to emphasize the appearance of periodicity, bifurcation and hysteresis of the flow.

A word of caution is in order here. When we will be claiming periodicity in time and symmetry in z of the flow field, it should be kept in mind that these results were obtained numerically and one cannot hope to prove here these properties in a rigorous mathematical sense. Enough care has been taken to check these properties, whenever such a claim is made, to go beyond graphical representations. Numbers were checked manually up to five significant figures to supplement the powerful flow-visualization tools. The claims made here like 'symmetry is exact', etc. are subject to the intrinsic limitations of the numerical methods. A similar difficulty arises when the number of stagnation points is counted (e.g. Table 1). In a numerical method, one cannot resolve the flow field indefinitely and the possibility exists of the stagnation points in the corners, etc. where the flow is weak and the length scales may be small due to secondary vortices. Hence in the count of stagnation points here, we include only those in the bulk of the flow field.

In Figure 3 are shown the streamline patterns for $Re = 1$ and two values of Ra. Flow is steady for both the cases and is symmetrical about the mid z-plane, $z = 1.5$. At $Ra = 10{,}000$, there is only one stagnation point, but at $Ra = 100{,}000$, the flow divides into cell-like structures and there are nine stagnation points. At values of Ra still higher flow becomes unsteady. The influence of these two parameters is shown in Figure 4. When $Re = 0$, there is natural convection if $Ra > Ra(\text{crit})$. This critical value has been determined numerically to be 2559 ± 2. For smaller values of Ra, there is no motion and we have pure conduction. The value of $Ra(\text{crit})$ for a cube[10] was found to be 3386.75 ± 0.25. The present lower value for a SAR of 3 is to be expected. The flow remained steady up to $Ra = 3 \times 10^5$ and it was found to be turbulent at $Ra = 10^6$. When Ra is increased from $Ra(\text{crit})$ to 3×10^5, drastic changes occur in the vortex

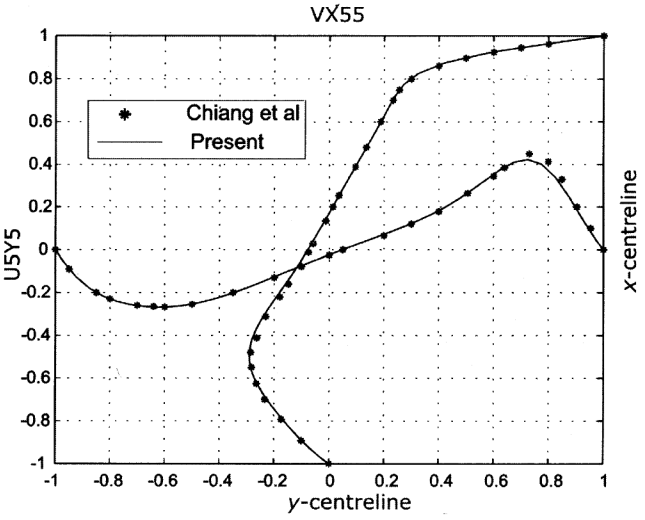

Figure 2. Velocity plots along the centreline of two axes showing comparison between data of Chiang *et al.*[9] and the present case for $Re = 400$ and $Ra = 0$.

Table 1. Number of stagnation points and closed streamlines for different combinations of Re and Ra in a rectangular parallelepiped of spanwise aspect ratio 3. $Pr = 7.0$

$Ra \rightarrow$ / $Re\downarrow$	Number of stagnation points (no. of closed loops)			
	0	10^4	4×10^4	5×10^4
1	3 (*)	1 (*)	–	1 (0)
50	3 (4)	3 (*)	1 (0)	–
100	1 (0)	1 (0)	–	1 (0)
200	1 (0)	1 (0)	–	1 (0)
400	1 (0)	1 (0)	–	1 (0)

*Because of the nearly 2D nature of the flow, streamlines in the $z = 1.5$ plane are almost closed. Hence it is difficult to conclude anything by numerical tools.

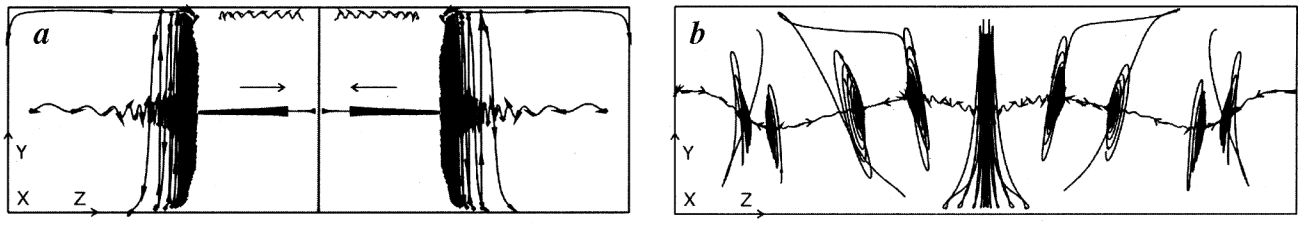

Figure 3. Top view showing vortices for $Re = 1$ and two different Ra. ***a***, Primary and secondary vortices (DSE) for $Ra = 10{,}000$. ***b***, Skeletal structure of vortices for $Ra = 100{,}000$. There are nine stagnation points.

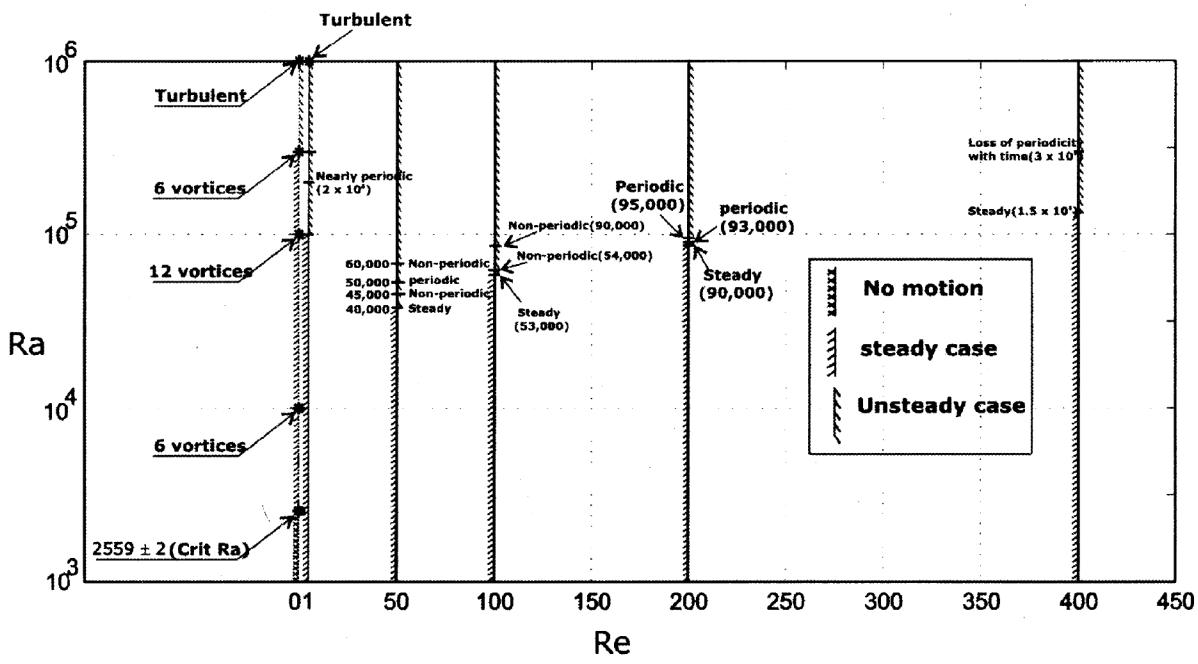

Figure 4. Plot of Ra versus Re showing periodic, aperiodic and turbulent cases. $Pr = 7.0$.

Table 2. Location of stagnation points in a rectangular parallelepiped of spanwise aspect ratio 3 for $Ra = 0$ and different Re

Reynolds number (Re)	Left half			Central plane ($z_s = 1.5$)	
	x_s	y_s	z_s	x_s	y_s
1	0.23524	0.50166	1.0320	0.23602	0.50168
50	0.24150	0.57640	1.1770	0.24150	0.57640
100	–	–	–	0.26180	0.61490
200	–	–	–	0.33230	0.59600
400	–	–	–	0.40880	0.53670

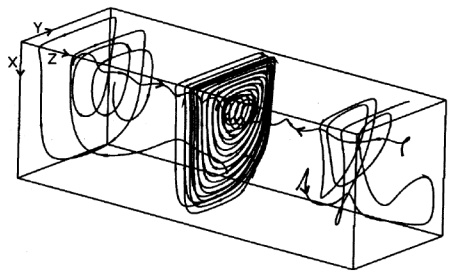

Figure 5. Streamline plots at time $\tau = 60.18675$ for $Re = 50$ and $Ra = 50{,}000$.

structure even though the flow remains steady. No attempt has been made to identify the boundaries of different regimes, which may not even be sharp. Details of this flow are available in Deshpande[7] and Deshpande and Srinidhi[11].

When $Ra = 0$, we get the other limiting case and motion is present for all the values of Re. This is the classical lid-driven cavity case[12]. Flow is steady for all the values of Re studied. Secondary vortices are present along the two spanwise bottom corners. For example, Figure 3 *a* shows one secondary eddy, even though in that case $Ra \neq 0$. At $Re = 1$ (and $Ra = 0$), there are three stagnation points, one on the mid z-plane and the other two located symmetrically (Table 2). Table 2 can be used conveniently to imagine the qualitative change that takes place. We had difficulty in identifying the stagnation points at $Re = 0.1$, since the flow turns out to be almost 2D. Closed streamlines are rare in three-dimensional flows, but they do exist here (Table 1). Table 1 is a summary of the drastic changes in the flow structure that take place when Re and also Ra are varied.

Table 3. z-location of stagnation point(s) at different phase locations in the periodic flow at $Re = 50$ and $Ra = 50{,}000$ in a rectangular parallelepiped of spanwise aspect ratio 3. $Pr = 7.0$

Point	Time	Relative time (%)	z_s	Comment
1	57.58225	0.000	1.88	Two left stagnation points just degenerate and disappear at $z = 1.5$
2	58.30025	9.978	1.864	Single stagnation point
3	58.80000	16.924	1.820	
4	59.08225	20.846	1.789	
5	59.88675	32.027	1.635	
8	60.18675	36.196	1.540	
10	60.38675	38.976	1.473	
11	60.46925	40.122	1.453	
12	60.55150	41.265	1.454	
14	60.66175	42.798	1.478	
15	60.68900	43.176	1.485	w–z plot has a point of inflection
16	60.71650	43.558	1.282, 1.483, 1.728	Three stagnation points
18	60.87675	45.786	1.046, 1.482, 1.979	
19	60.96400	46.998	1.023, 1.468, 1.995	
20	61.04675	48.148	1.027, 1.478, 1.976	
22	61.21150	50.437	1.057, 1.473, 1.936	
25	62.49575	68.286	1.066, 1.453, 1.926	
26	64.38675	94.566	1.086, 1.266, 1.907	Three stagnation points
27	64.77775	100.000	1.880	End of three stagnation points

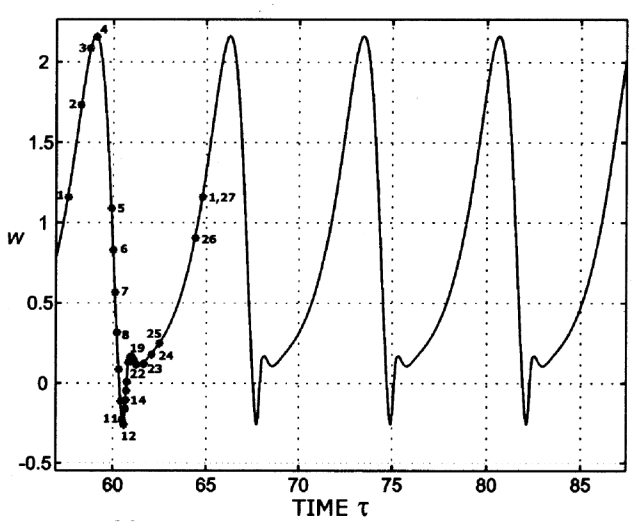

Figure 6. Velocity–time trace at (0.23750, 0.5, 1.5) for $Re = 50$ and $Ra = 50{,}000$. 1 to 27, indicate points that are being considered for the study.

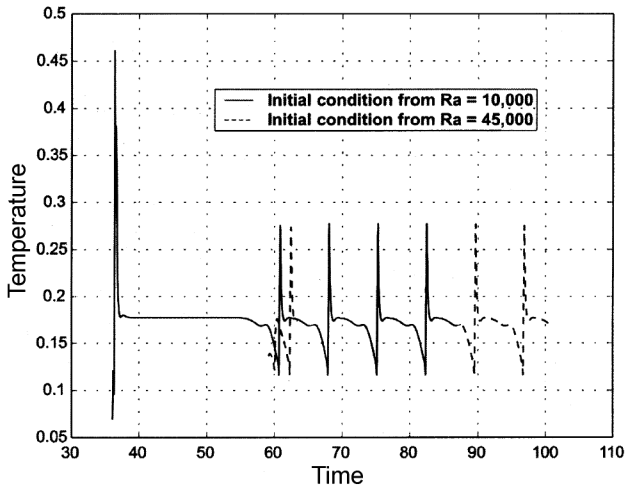

Figure 7. Temperature–time trace at (0.5, 0.41250, 1.5) for $Re = 50$ and $Ra = 50{,}000$ with two different initial conditions. Comparison showed that the same solution is retained even with change of initial condition.

Periodic flow at Reynolds number 50

At $Re = 50$, if Ra is increased gradually, the flow remains steady up to $Ra = 40{,}000$. Still there is a drastic change in the flow structure when Ra is increased from 10,000 to 40,000. As seen from Table 1, the number of stagnation points decreases from 3 to 1, accompanied by a change in flow direction. Figure 5 shows the streamline pattern at some instant and for $Ra = 50{,}000$. The flow is unsteady and unsymmetrical about the mid z-plane, which divides the flow into two primary vortices, one on each side. The flow in the vortex core is towards the mid z-plane. Outside the vortex core, the flow has to move towards the end planes. For this (Re, Ra) combination the flow was found to be periodic in time, as seen from the velocity–time trace in Figure 6. It is somewhat surprising that such a complex flow field involving secondary vortices and governed by nonlinear equations, can be periodic. This amounts to every variable at every point in the cavity changing periodically.

To investigate the robustness and reliability of this surprising periodic behaviour, some tests were conducted. Results of one such test are shown in Figure 7, where computations are started with different initial conditions to check if the same periodic flow for $Re = 50$, $Ra = 50{,}000$ is reached. The case with $Ra = 10{,}000$ as the initial condition is steady but that with $Ra = 45{,}000$ is unsteady and non-

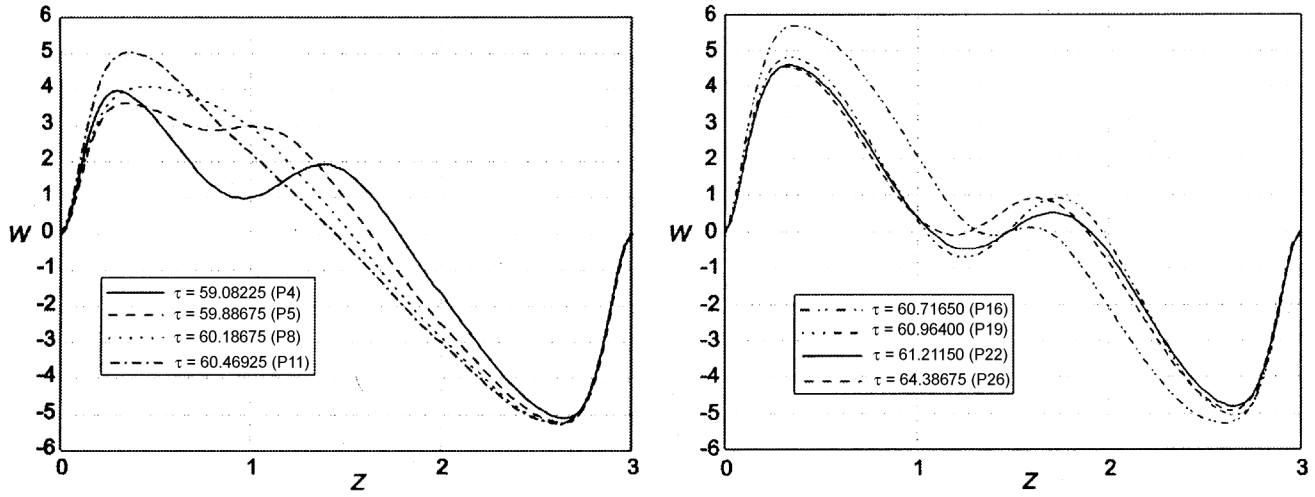

Figure 8. Plot showing w velocity along the vortex centre at different times in a single period for $Re = 50$ and $Ra = 50{,}000$.

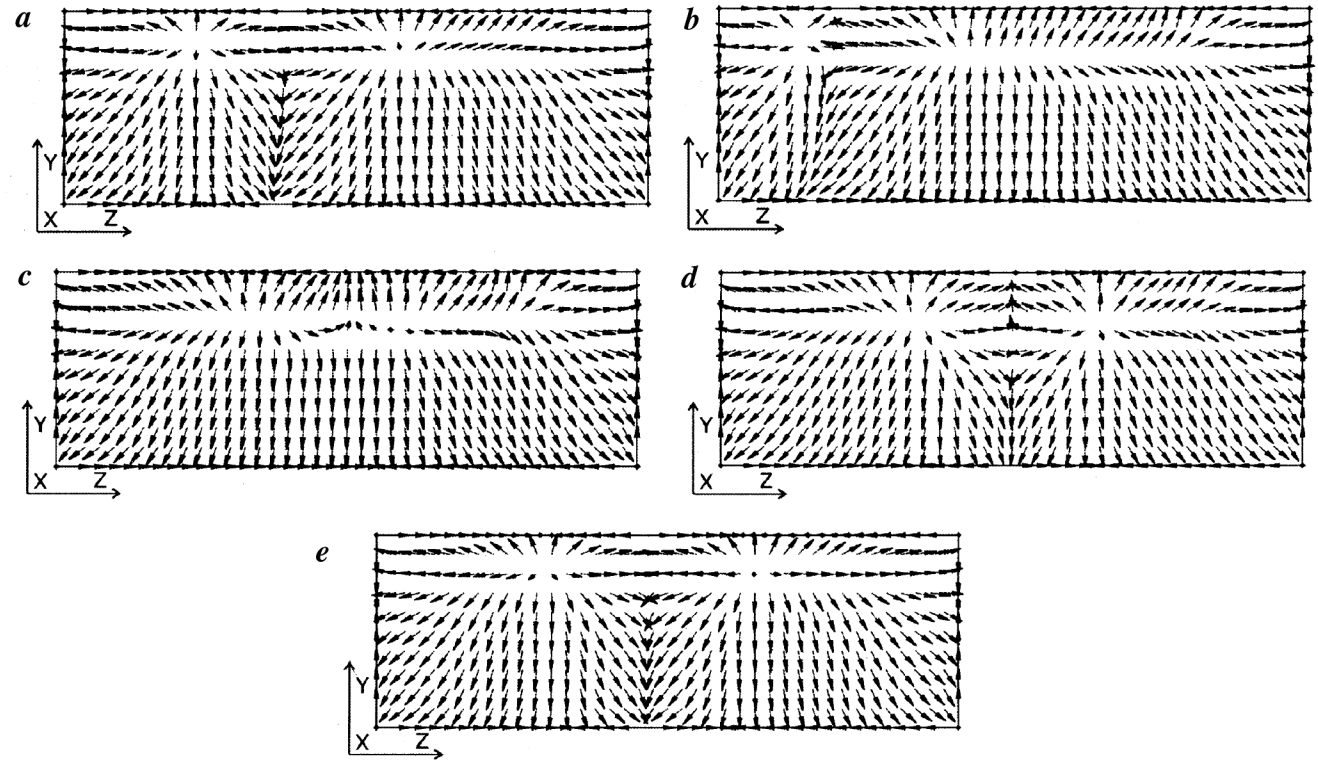

Figure 9. Velocity vector plots at $x = 0.95$ plane at different times in a single period for $Re = 50$ and $Ra = 50{,}000$. ***a***, $\tau = 59.08225$ (P4). ***b***, $\tau = 60.18675$ (P8). ***c***, $\tau = 60.46925$ (P11). ***d***, $\tau = 60.66175$ (P14). (***e***) $\tau = 64.38675$ (P26).

periodic. See that the second case quickly changes the period and falls in line, indicating the robustness of the flow. Another test will be described later.

Referring back to the periodic time trace in Figure 6, the period here is 7.1952 time units and points have been marked 1 to 27 to study changes during one cycle. Velocity profiles of w as a function of z along the vortex centre for different times are shown in Figure 8. The sign of this velocity component is an important indicator of the axial motion of the vortices and hence this picture describes the overall flow in a qualitative sense. The location of the stagnation point is given in Table 3. For points 1 to 15, there is only one point where the w component becomes zero on the z-centreline. For points 16 to 26, we have three such points. This periodic phenomenon is not symmetric in z. Since there is no speciality about one side of the cavity, another solution

should be possible which is also periodic and is the mirror reflection of the present solution in z. We may refer to the multiplicity of the solutions found in natural convection inside a cube[10,13] and its symmetric variants. The velocity vector plots on plane $x = 0.95$ which is close to the cavity bottom plate are shown in Figure 9. Heat flux plots at the bottom plate at these five points (i.e. times in the periodic cycle) are shown in Figure 10. Figures 8–10 clearly indicate how the flow is oscillating non-symmetrically about the mid z-plane unlike, as we will see, the next case for $Re = 200$.

To investigate how reliable is the periodicity, the velocity and temperature profiles over an entire line in the cavity were checked for exact repetition after a complete cycle. One such plot is shown in Figure 11 *a*. We see that the

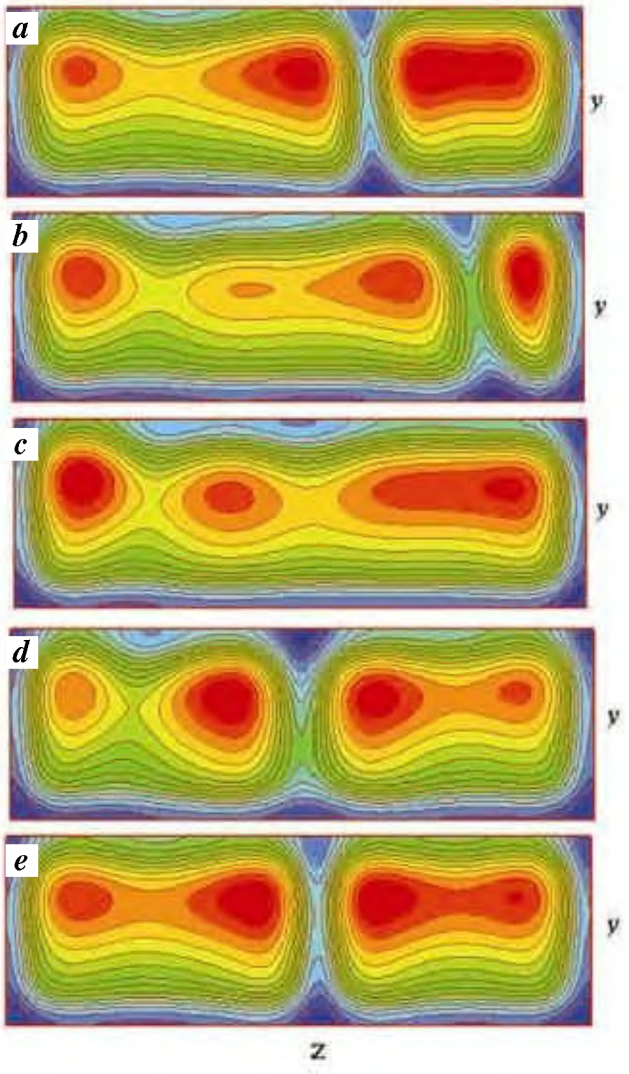

Figure 10. Heat flux contours at bottom plate $x = 1$ at different times for $Re = 50$ and $Ra = 50{,}000$. Minimum and maximum values of heat flux are shown in brackets. ***a***, $\tau = 59.08225$ (P4). (min = 1.163, max = 9.171). ***b***, $\tau = 60.18675$ (P8). (min = 1.165, max = 8.942). ***c***, $\tau = 60.46925$ (P11). (min = 1.101, max = 8.413). ***d***, $\tau = 60.66175$ (P14). (min = 1.161, max = 9.134). ***e***, $\tau = 64.38675$ (P26). (min = 1.166, max = 9.061).

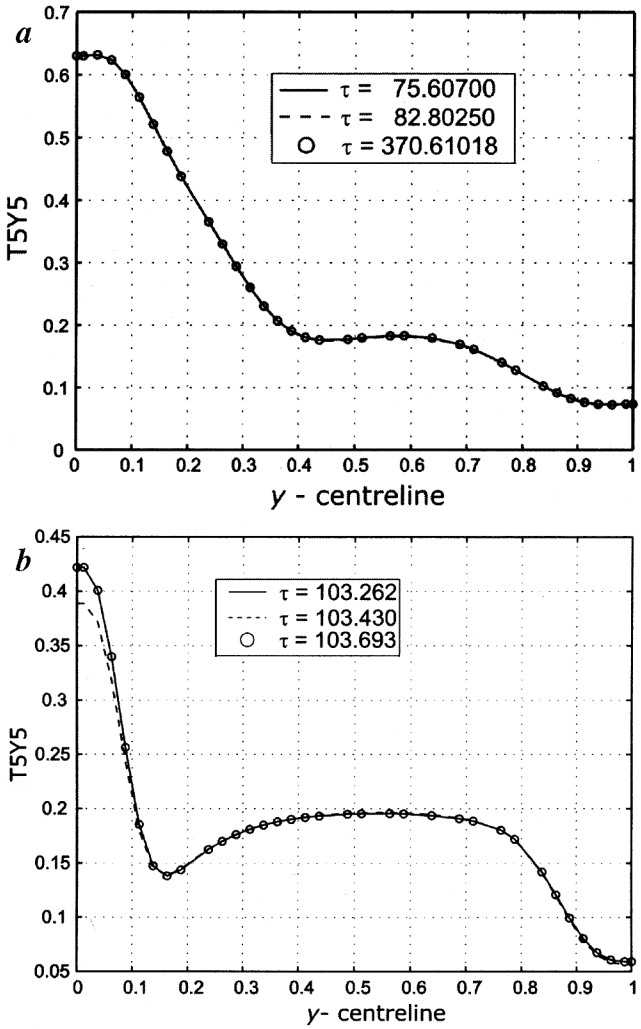

Figure 11. Comparison of temperature profiles of two periodic solutions obtained by two different Re and Ra combinations. ***a***, Comparison between three cycles (2nd, 3rd and 43rd) to check for stable periodicity at $Re = 50$ and $Ra = 50{,}000$. ***b***, Comparison between three consecutive peaks in a single period at $Re = 200$ and $Ra = 94{,}800$. $T = 0.4316$.

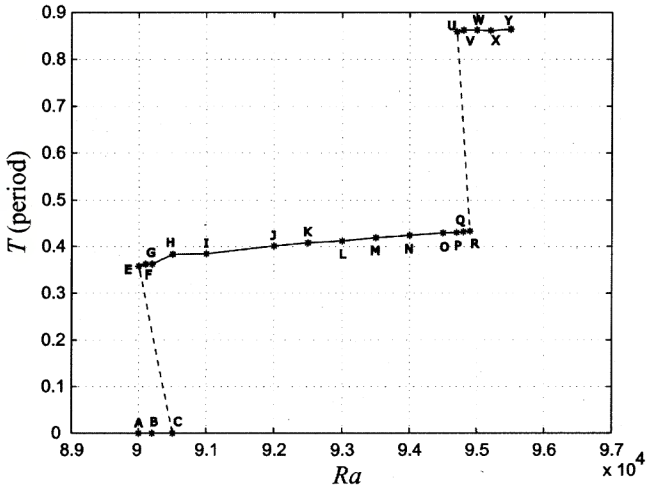

Figure 12. Period T plotted as a function of Ra for $Re = 200$ and $Pr = 7.0$. Dashed lines indicate unstable solution.

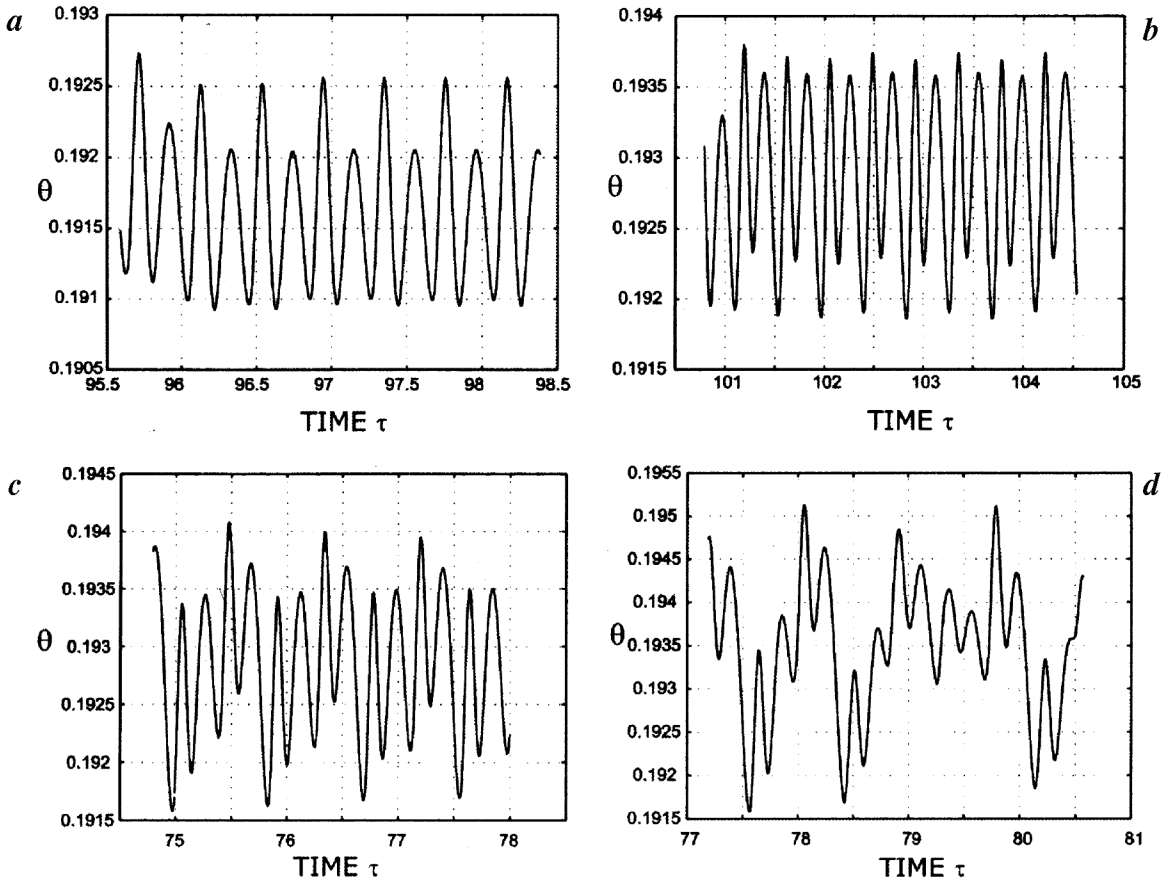

Figure 13. Temperature–time trace at the point (0.5, 0.41250, 1.5) for $Re = 200$ and $Pr = 7.0$ and different Ra. Points indicated in brackets correspond to same points in Figure 6. ***a***, $Ra = 92{,}500$ (point K); ***b***, $Ra = 94{,}800$ (point Q); ***c***, $Ra = 94{,}800$ (point V) and ***d***, $Ra = 95{,}800$.

entire temperature profile repeats exactly after one and even 41 cycles assuring exact, stable periodicity. Similar checks were carried out for other variables along different lines. When Ra is increased to a slightly higher value of 60,000, periodicity is lost. For a much higher value of $Ra = 10^6$ the flow resembles turbulence[14].

Periodic flow at Reynolds number 200

Now we take up another case of $Re = 200$, where periodicity is observed in the neighbourhood of $Ra = 93{,}000$. We also see here the phenomena of bifurcation, period doubling and hysteresis. Referring to Figure 11 *b* for $Re = 200$ and $Ra = 94{,}800$, we see exact replication of the temperature profile after period $T = 0.4316$. In Figure 12, time period T of the flow is plotted as a function of parameter Ra. Up to $Ra = 90{,}500$ corresponding to point C on the graph, the flow, is steady leading to $T = 0$. An increase in Ra leads to the appearance of unsteady periodic flow, where period T increases gradually with its value being around 0.4. Thus a bifurcation has taken place from an equilibrium solution (steady) to another one (periodic). A subsequent bifurcation around $Ra = 95{,}000$ leads to period doubling and the next equilibrium solution moves along UVWXY. The period T at $Ra = 94{,}700$ changes from 0.430 (at point P) to 0.859 (point U) and at $Ra = 94{,}800$, from 0.4316 (Q) to 0.8624 (V). These values are tabulated in Deshpande and Srinidhi[2]. We may add here that the periodic case for $Re = 200$ on both these branches is associated with exact symmetry about the mid z-plane at every instant. Around both of these bifurcations we see an overlap of the curves, indicating a hysteresis in the flow. A further increase in Ra beyond point Y leads to the loss of periodicity. The top branch in Figure 12 is shorter than the middle branch. All these features are similar to elementary model bifurcations[15]. It may be noted that every point A to Y on the branches in Figure 12, corresponds to an equilibrium solution.

It is interesting to see that the time traces and the velocity and temperature profiles for these cases give us a clue about the mechanism of bifurcation. In Figure 13, time traces for θ are shown for four cases of Ra: point K, $Ra = 92{,}500$; point Q, $Ra = 94{,}800$; point V, $Ra = 94{,}800$ on the top branch and finally for a non-periodic case $Ra = 95{,}800$. This non-periodicity is associated with the loss of symmetry in z. These time traces indicate how a small change in Ra may

lead to a drift to another branch in the bifurcation diagram. Specially notice Figure 13 *b* and *c*, which is for the same value of $Ra = 94{,}800$. Periodicity is lost for $Ra = 95{,}800$. Velocity and temperature profiles indicate a slight local drift, but agree in most of the locations when period doubling takes place. Figure 11 *b* is a temperature profile for an intermediate peak point $\tau = 103.430$ inside a period. The heat flux plots for the bottom plate in Figure 14, show drastic variation in quantity. These plots were made at some arbitrary values of time. The patterns for the same value of $Ra = 90{,}500$ (frames *a* and *b*) and also $Ra = 94{,}800$ (frames *c* and *d*), are qualitatively different, but both the sets correspond to periodic flows that are also symmetrical in *z*. In frame *e* for $Ra = 95{,}700$, periodicity and symmetry are lost.

Now we move to another interesting comparison with a relatively high value of $Ra = 10^6$. The first frame in Figure 15 with $Re = 0$ corresponds to natural convection. The flow seems to get organized into small cells as *Re* is increased. The average Nusselt number (Nu) variation as a function of *Ra* for different *Re* is shown in Figure 16. These plots do not give a clue to the drastic changes that take place in

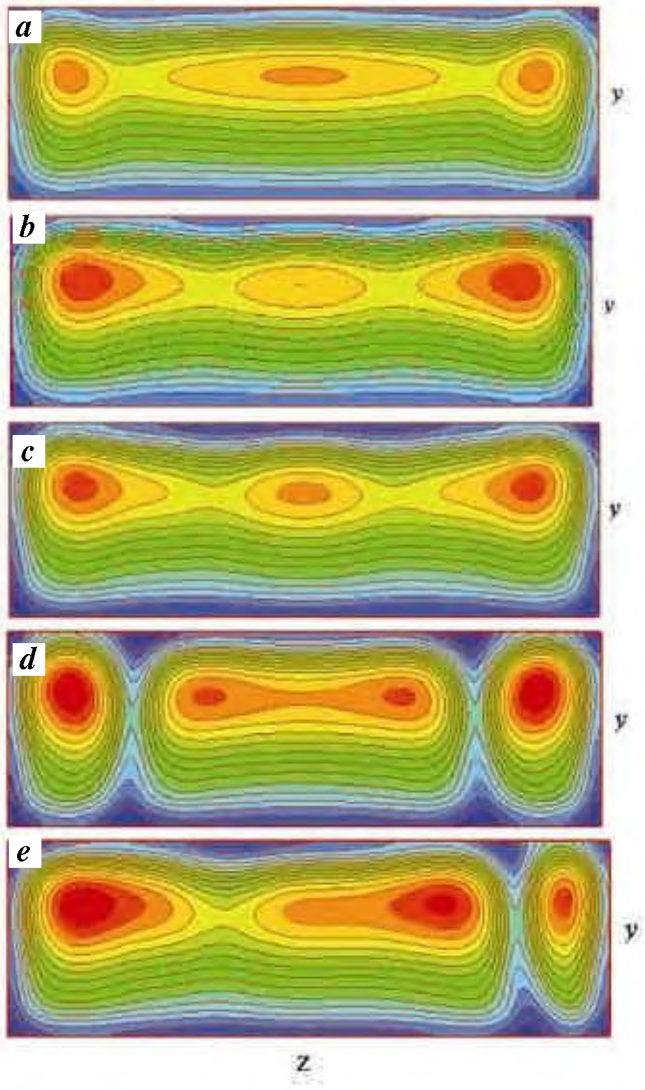

Figure 14. Heat flux contours at bottom plate $x = 1$ for $Re = 200$ and three values *Ra*. Minimum and maximum values of heat flux are shown in brackets. ***a***, $Ra = 90{,}500$ (point C). (min = 1.337, max = 13.575). ***b***, $Ra = 90{,}500$ (point H). (min = 1.337, max = 13.575). ***c***, $Ra = 94{,}800$ (point Q). (min = 1.337, max = 13.575). ***d***, $Ra = 94{,}800$ (point V). (min = 1.385, max = 14.782). ***e***, $Ra = 95{,}700$ (min = 1.074, max = 14.340).

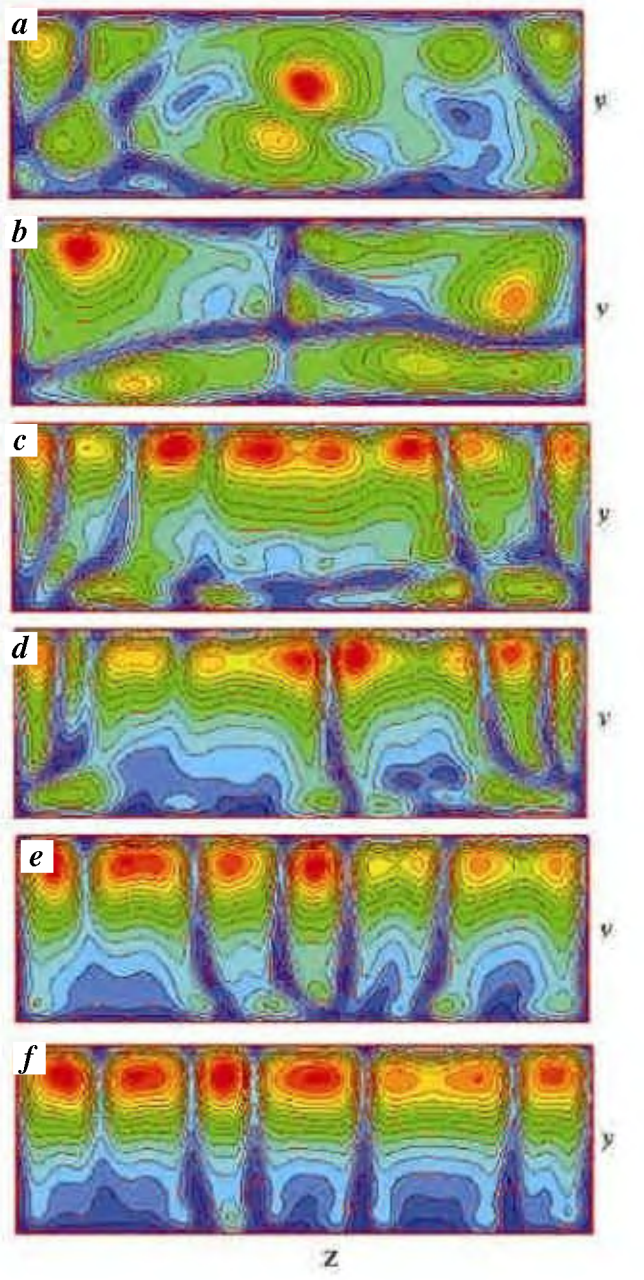

Figure 15. Heat flux contours at bottom plate $x = 1$ for $Ra = 10^6$ and different *Re*. Minimum and maximum values of heat flux are shown in brackets. ***a***, $Re = 0$ at $\tau = 11.14425$ (min = 1.262, max = 22.751). ***b***, $Re = 1$ at $\tau = 77.08225$ (min = 1.318, max = 23.486). ***c***, $Re = 50$ at $\tau = 5.2221$ (min = 1.111, max = 24.696). ***d***, $Re = 100$ at $\tau = 3.42205$ (min = 1.424, max = 30.315). ***e***, $Re = 200$ at $\tau = 67.2901$ (min = 1.409, max = 35.316). ***f***, $Re = 400$ at $\tau = 47.99005$ (min = 1.232, max = 29.952).

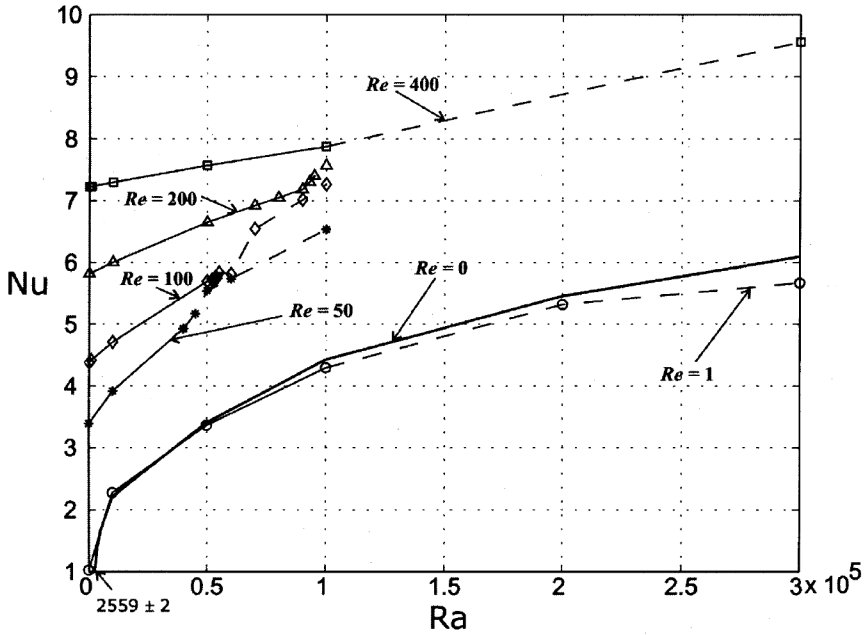

Figure 16. Dependence of *Nu* on *Ra* for different *Re*. Dashed lines indicate unsteady flow and values of *Nu* are taken at some arbitrary instant.

the flow. Attention is specially drawn to the unusual case of $Re = 1$, where this slight forcing (compared to $Re = 0$) may even decrease the average heat flux.

Conclusion

We have observed periodic mixed convection even when the boundary conditions applied were steady. Periodicity may or may not be associated with symmetry in z. When it was associated with symmetry, loss of periodicity and loss of symmetry were observed to occur together. The classical features of dynamical systems like bifurcation, hysteresis and period doubling usually observed in phase space are seen here in physical space itself. These results, apart from being of fundamental importance, have practical relevance[16] in areas like material processing and other engineering applications.

1. Deshpande, M. D. and Srinidhi, B. G., Mixed convection in a lid-driven three-dimensional cavity, NAL Project Document PD CF 0413, 2004.
2. Deshpande, M. D. and Srinidhi, B. G., Bifurcation, period doubling and hysteresis in mixed convection in a cavity, NAL Project Document PD CF 0507, 2005.
3. Prasad, A. K. and Koseff, J. R., Combined forced and natural convection heat transfer in a deep lid-driven cavity flow. *Int. J. Heat Fluid Flow*, 1996, **17**, 460–467.
4. Chandrasekhar, S., In *Hydrodynamic and Hydromagnetic Stability*, Clarendon Press, Oxford, 1961.
5. Harlow, F. H. and Welch, J. E., Numerical calculation of time-dependent viscous incompressible flow of fluid with free surface. *Phys. Fluids*, 1965, **8**, 2182–2189.
6. Kawamura, T., Takami, H. and Kuwahara, K., Computation of high Reynolds number flow around a circular cylinder with surface roughness. *Fluid Dyn. Res.*, 1986, **1**, 145–162.
7. Deshpande, M. D., Free convection in a three-dimensional cavity, NAL Project Document PD CF 0303, 2003.
8. Stuart, J. T., On the cellular patterns in thermal convection. *J. Fluid Mech.*, 1964, **18**, 481–498.
9. Chiang, T. P., Hwang, R. R. and Sheu, W. H., Finite volume analysis of spiral motion in a rectangular lid-driven cavity. *Int. J. Num. Methods Fluids*, 1996, **23**, 325–346.
10. Deshpande, M. D., Natural convection in a cubical cavity: Case of multiple solutions, NAL Project Document PD CF 0305, 2003.
11. Deshpande, M. D. and Srinidhi, B. G., Natural convection in a cavity of large aspect ratio, NAL Project Document PD CF 0312, 2003.
12. Shankar, P. N. and Deshpande, M. D., Fluid mechanics in the driven cavity. *Annu. Rev. Fluid Mech.*, 2000, **32**, 93–136.
13. Deshpande, M. D. and Srinidhi, B. G., Further studies on multiple solutions in natural convection in a cuboid, NAL Project Document PD CF 0315, 2003.
14. Deshpande, M. D. and Srinidhi, B. G., Mixed convection in a cavity: Generation of periodic and unsteady convection, NAL Project Document PD CF 0502, 2005.
15. Hale, J. and Kocak, H., *Dynamics and Bifurcations*, Springer-Verlag, 1991.
16. Jaluria, Y., Fluid flow phenomena in material processing – The 2000 Freeman Scholar Lecture. *J. Fluids Eng.*, 2001, **123**, 173–210.

ACKNOWLEDGEMENT. We thank the anonymous referee for making constructive suggestions.

Received 4 August 2005; revised accepted 28 September 2005